JACS
JOURNAL OF THE AMERICAN CHEMICAL SOCIETY
pubs.acs.org/JACS
Communication

Kinetic Control in the Synthesis of a Möbius Tris((ethynyl)[5]helicene) Macrocycle Using Alkyne Metathesis

Xing Jiang,[▽] Summer D. Laffoon,[▽] Dandan Chen,[▽] Salvador Pérez-Estrada, Andrew S. Danis, Joaquín Rodríguez-López, Miguel A. Garcia-Garibay,* Jun Zhu,* and Jeffrey S. Moore*

Cite This: https://dx.doi.org/10.1021/jacs.0c01430

ABSTRACT: The synthesis of conjugated Möbius molecules remains elusive since twisted and macrocyclic structures are low-entropy species sporting their own synthetic challenges. Here we report the synthesis of a Möbius macrocycle in 84% yield via alkyne metathesis of 2,13-bis(propynyl)[5]helicene. MALDI-MS, NMR spectroscopy, and X-ray diffraction indicated a trimeric product of twofold symmetry with *PPM/MMP* configurations in the helicene subunits. Alternatively, a threefold-symmetric *PPP/MMM* structure was determined by DFT calculations to be more thermodynamically stable, illustrating remarkable kinetic selectivity for this alkyne metathesis cyclooligomerization. Computational studies provided insight into the kinetic selectivity, demonstrating a difference of 15.4 kcal/mol between the activation barriers for the *PPM/MMP* and *PPP/MMM* diastereodetermining steps. Computational (ACID and EDDB) and experimental (UV−vis and fluorescence spectroscopy and cyclic voltammetry) studies revealed weak conjugation between the alkyne and adjacent helicene groups as well as the lack of significant global aromaticity. Separation of the *PPM* and *MMP* enantiomers was achieved via chiral HPLC at the analytical scale.

Dynamic covalent chemistry (DCC) is a powerful synthetic strategy for assembling complex structures via reversible reactions from simple building blocks. Such reactions, including alkyne metathesis, imine condensation, disulfide exchange, and boronic acid condensation, have facilitated the preparation of organic architectures such as macrocycles, catenanes, cages, and extended frameworks.[1] Thermodynamically controlled DCC reactions enable error correction of intermediates along multiple reaction pathways, offering facile access to intricate connectivity and topology beyond the reach of conventional synthesis. We and others have developed alkyne metathesis cyclooligomerization[2] as a useful method for the efficient preparation of conjugated and shape-persistent molecules where stepwise synthetic strategies have fallen short.[3]

Limited examples of Möbius structures have been reported because of the challenges associated with synthesizing macrocycles and twisted structures.[4] Among them, many feature porphyrinoid scaffolds, in part because of the heightened structural rigidity offered by pyrrole moieties.[5] Two non-porphyrinoid Möbius structures with writhe-bearing subunits have been recently reported by Rissanen, Herges, and Durola (Figure 1) with different synthetic strategies regarding the order of macrocyclization and writhe formation.[6] While their successes are inspiring to theoretical and experimental chemists, both synthetic routes are lengthy with low overall yields (~1%). Very recently, Tanaka synthesized Möbius [*n*]cycloparaphenylene (CPP) analogues utilizing [2 + 2 + 2] cyclization with great enantioselectivity yet low overall yield.[7] To circumvent the limitations associated with stepwise macrocycle construction, we investigated a DCC-based assembly of simple monomers into molecular Möbius strips in a single step. We pursued a route toward a fully conjugated

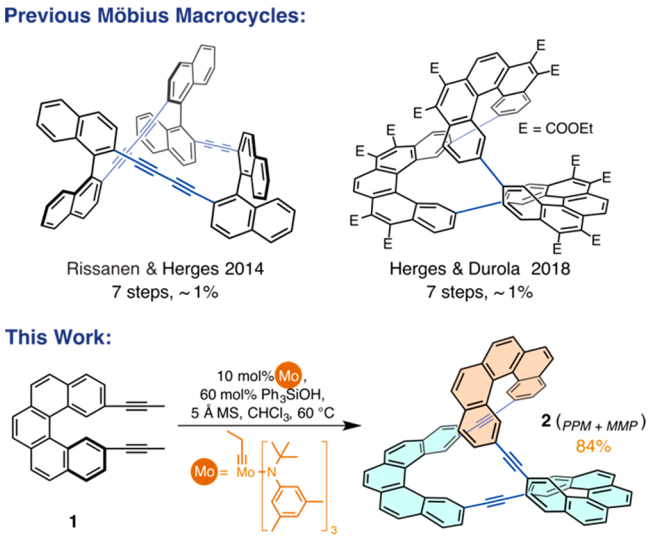

Figure 1. Structures of recently reported Möbius molecules and efficient synthesis via alkyne metathesis in this work.

structure via alkyne metathesis given the influence that Möbius topology holds over the aromaticity of an annulene.[8,9] Herein

Received: February 10, 2020
Published: March 25, 2020

https://dx.doi.org/10.1021/jacs.0c01430
J. Am. Chem. Soc. XXXX, XXX, XXX−XXX

we report the efficient synthesis of Möbius macrocycle **2** from the metathesis of 2,13-bis(propynyl)[5]helicene **1**.

Bis(propynyl)[5]helicene **1**, prepared from 2,13-dibromo[5]helicene[10] in 90% yield, features a low inversion barrier of 25.6 kcal/mol, similar to that of the parent [5]helicene[11] (23.4 kcal/mol; see Table S2). The dynamic helicity makes **1** an ideal candidate for cyclooligomerization, as chirality matching is allowed in the final ring closure step. Compound **1** was first subjected to alkyne metathesis conditions with 10 mol % $[EtC{\equiv}Mo(OSiPh_3)_3]$ at room temperature and 5 mM in $CHCl_3$. MALDI-MS analysis of the crude reaction mixture revealed that in addition to unconsumed starting material, ring-opened dimer, and higher-molecular-weight oligomers, a peak at m/z 900.2838 (Figure 2A) corresponding to the ring-closed trimer **2** was observed.

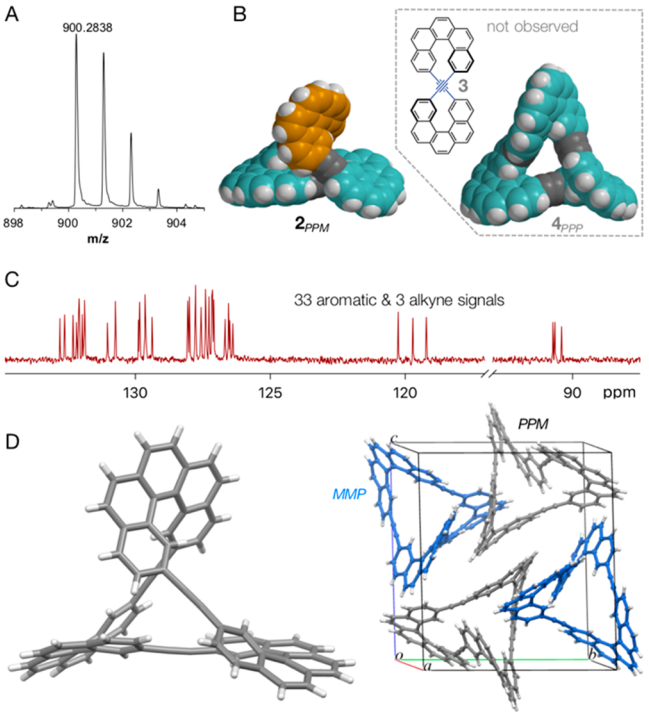

Figure 2. (A) MALDI-TOF mass spectrometry established the formation of a ring-closed trimeric species. (B) Space-filling models of DFT-calculated structures of $\mathbf{2}_{PPM}$ and $\mathbf{4}_{PPP}$. (C) ^{13}C NMR spectrum showing 36 carbon signals. (D) Crystal structure of $\mathbf{2}_{PPM}$ (left) and the unit cell (right). Solvent molecules have been omitted for clarity.

The ring-closed dimer **3** was never observed. Under the above reaction conditions, the trimeric product was formed in 23% yield as determined by NMR spectroscopy. To limit the formation of oligomeric products, we diluted the reaction mixture to 1 mM and increased the temperature to 40 °C, obtaining the ring-closed trimer in 38% NMR yield. Increasing the temperature to 60 °C at the same reaction concentration led to the optimized conditions, giving an 84% NMR yield. The solvent effect was also briefly explored, and reactions in toluene gave significantly lower yields at elevated temperatures due to competing precipitation (Table S1).

With regard to the symmetry of the macrocyclic product, four stereoisomers are possible, namely, the *PPM* and *MMP* enantiomeric pair of **2** and the *PPP* and *MMM* enantiomeric pair of **4** (Figure 2B). Both diastereomers are twisted structures with Möbius topology. The *PPP*/*MMM* pair features threefold symmetry and is triply twisted, while the *PPM*/*MMP* pair is C_2-symmetric and singly twisted. Single-point energy calculations (M06-2X, B3LYP, or PBE0 functional with the def2-TZVP basis set; Table S3) showed that **2** is less stable than **4** by 1−2 kcal/mol, suggesting that **4** is the thermodynamically favored product. However, the ^{13}C NMR spectrum of the product is consistent with the exclusive formation of **2,** showing 33 aromatic and three alkynyl carbon resonances (Figure 2C). The unexpected kinetic selectivity and the *PPM*/*MMP* stereochemistry of the product were confirmed by X-ray diffraction (XRD) of single crystals grown from a hot ethyl acetate solution. The crystal structure of **2** was solved in the orthorhombic $P2_1/n$ space group, with two pairs of *PPM*/*MMP* enantiomers in each unit cell (Figure 2D). The XRD structure is very close to the DFT-minimized structure, except that two of the three triple bonds deviate slightly from linearity (average bond angles of 175°, 176°, and 178°).

Since DCC reactions are typically under thermodynamic control, we were surprised that the less stable product **2** was formed exclusively in the reaction. In fact, thermodynamic driving forces are typically the sole factors considered when planning a DCC synthesis. To elucidate the origin of the kinetic selectivity, DFT calculations (B3LYP/6-31G(d)/SDD) of the intermediates and transition states leading to structures $\mathbf{2}_{PPM}$ and $\mathbf{4}_{PPP}$ were performed (Figure 3). The rate-determining step in both pathways is the initial formation of the metallacyclobutadiene (**TS1**). The activation energy for $\mathbf{TS1}_{PPP}$ formation is 37.0 kcal/mol, whereas the barrier for $\mathbf{TS1}_{PPM}$ formation is 21.6 kcal/mol. The 15.4 kcal/mol difference in activation energy accounts for the remarkable kinetic control in the synthesis. Notably, a single metallacyclobutadiene intermediate $\mathbf{IM}_{PPM}$ was located after $\mathbf{TS1}_{PPM}$, which quickly undergoes cycloreversion to give $\mathbf{2}_{PPM}$. This contrasts with the canonical observation of two discrete metallacyclobutadiene intermediates ($\mathbf{IM1}_{PPP}$ and $\mathbf{IM2}_{PPP}$) following the first transition state ($\mathbf{TS1}_{PPP}$) as observed for $\mathbf{4}_{PPP}$. $\mathbf{TS2}_{PPM}$ was difficult to locate, most likely because of a small energy difference (an early transition state according to the Hammond postulate) between $\mathbf{IM}_{PPM}$ and $\mathbf{TS2}_{PPM}$ (Figure S24). The free energy change from $\mathbf{TS1}_{PPM}$ to $\mathbf{2}_{PPM}$ is −38.2 kcal/mol, which is consistent with the observation that **2** is kinetically stable under metathesis conditions in the presence of excess 1-phenyl-1-propyne (Figure S17).

Our experimental and computational studies illustrate unique kinetic sensitivity of alkyne metathesis, particularly for the preparation of rigid structures. This results from the strained four-membered metallacycles in the intermediates and transition states leading to product and their significant deviation from linearity. Specifically, a significantly higher level of bond angle distortion was observed in $\mathbf{TS1}_{PPP}$ (138.7° and 117.4°) than in $\mathbf{TS1}_{PPM}$ (147.3° and 117.4°) (from $C_{Ar}-C_{sp}-Mo$ and $C_{Ar}-C_{sp}-C_{sp}$, respectively), while no apparent difference was noticed in terms of dihedral angle or bond length (Figure S23). Therefore, seemingly stable and unstrained products may have surprisingly high energy barriers when constructed with alkyne metathesis. In the synthesis of **2**, such kinetic selectivity affords complete diastereocontrol.

The optical properties of **2** were explored to probe its electronic structure. The UV−vis and fluorescence excitation spectra of **2** are slightly red-shifted compared with those of **1**, while the emission spectra are nearly identical (Figure 4). We attribute this to weak conjugation among the three helicene subunits in **2** and an increase in oscillator strength for the S_0-

https://dx.doi.org/10.1021/jacs.0c01430
J. Am. Chem. Soc. XXXX, XXX, XXX−XXX

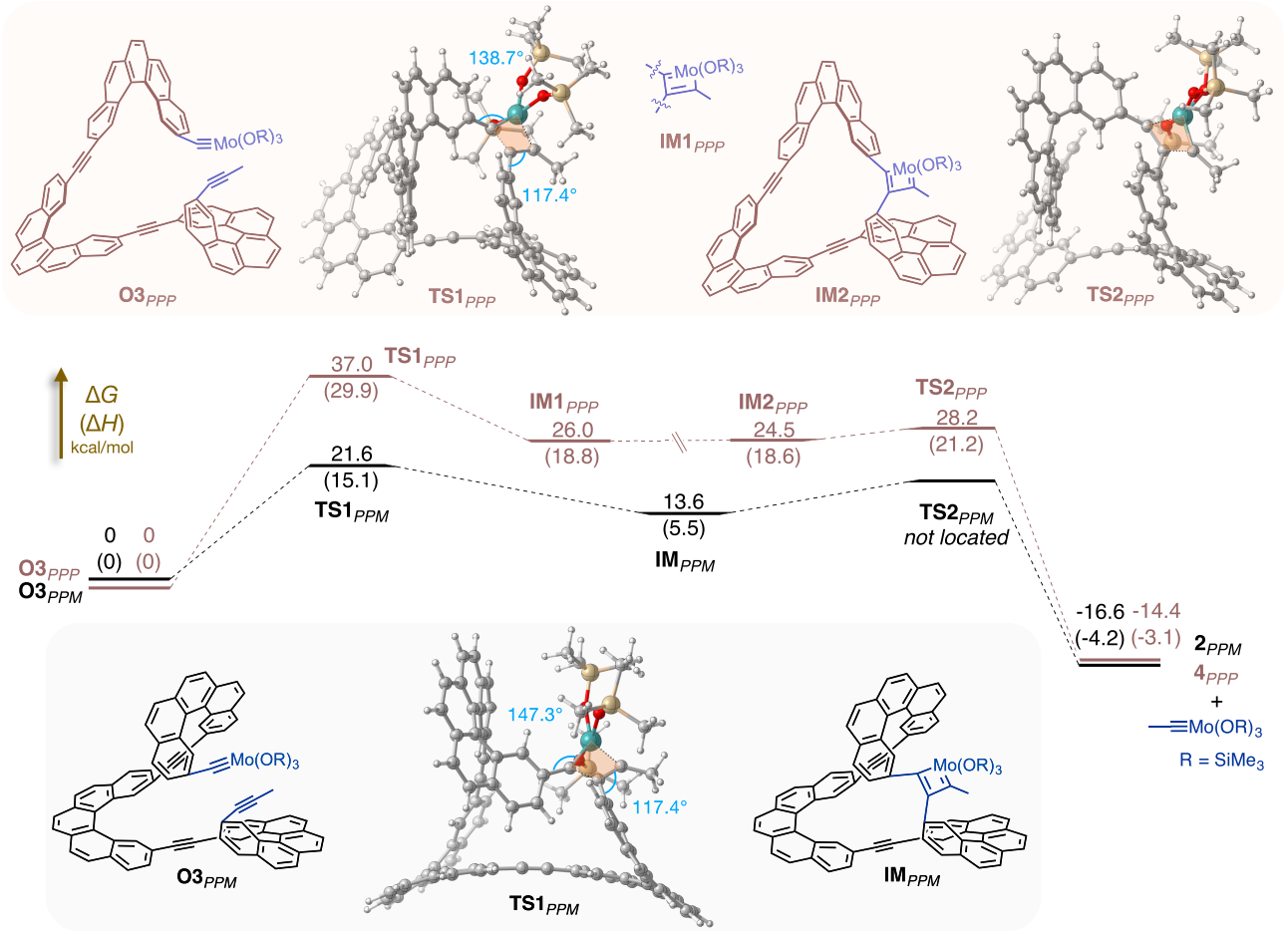

Figure 3. DFT (B3LYP/6-31G(d)/SDD)-calculated relative Gibbs free energies and (in parentheses) enthalpies of intermediates and transition state structures in the formation of $\mathbf{2}_{PPM}$ and $\mathbf{4}_{PPP}$. Energies in both pathways are relative to the open trimers $\mathbf{O3}_{PPM}$ and $\mathbf{O3}_{PPP}$, respectively. The SMD solvation model (CH_3Cl) was used in the calculation. The rate-determining step in both pathways is the formation of the metallacyclobutadiene (**TS1**). A simplified Me_3SiO- ligand was used in the calculation. The transition state structures were rendered in CYLview.[12] The metallacyclobutadiene structures are highlighted in orange, and bond angles in **TS1** are labeled in blue.

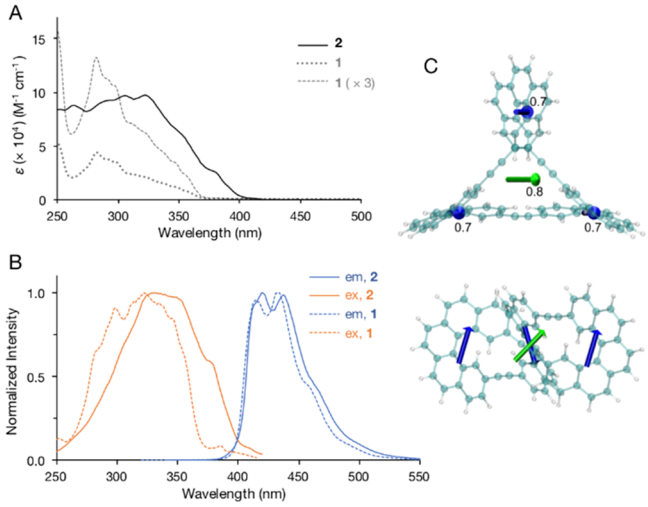

Figure 4. (A) UV−vis and (B) fluorescence spectra of **1** and **2** in DCM. (C) The S_0-S_1 electric transition dipole moments (μ_e) of $\mathbf{2}_{PPM}$ (green arrow; the contribution of the acetylene carbons is not included) and the three helicene segments (blue arrows). Their absolute values are labeled (unit: debye).

S_1 transition in going from **1** to **2**. The S_0-S_1 transition and other low-energy transitions of **1** are symmetry-forbidden and extremely weak, but the oscillator strengths of the same transitions are higher for **2** (Table S5). The S_0-S_1 electric transition dipole moment of $\mathbf{2}_{PPM}$ resembles the sum of those of the three helicene units, and the spatial arrangement of transition dipole moments of *P*- and *M*-helicene enables the otherwise forbidden transition (Figure 4C). The increased oscillator strength justifies the increased quantum yield of **2** over **1** (2.7% and 1.3%, respectively). To further probe the electronic structure, comparative voltammetric measurements of **1** and **2** were performed (Figures S18−S22). For the reduction process, the magnitude of the normalized peak currents (with respect to concentration and redox equivalents) indicates a single three-electron voltammetric wave for **2** (Figure S22). The lack of stepwise behavior suggests that three electrons are accepted in redox centers that act independently of each other.[13] This strengthens conclusions regarding the additive behavior of the helicene units.

The photophysical and electrochemical properties described above are consistent with our theoretical interrogations of $\mathbf{2}_{PPM}$. The electron density of delocalized bonds (EDDB) plot shows that one set of *p* orbitals of the alkynes are parallel to the *p* orbitals of the adjacent helicenes, indicating significant

https://dx.doi.org/10.1021/jacs.0c01430
J. Am. Chem. Soc. XXXX, XXX, XXX−XXX

conjugation between those moieties, albeit less pronounced than the delocalization within the helicene units (Figure 5A, π-

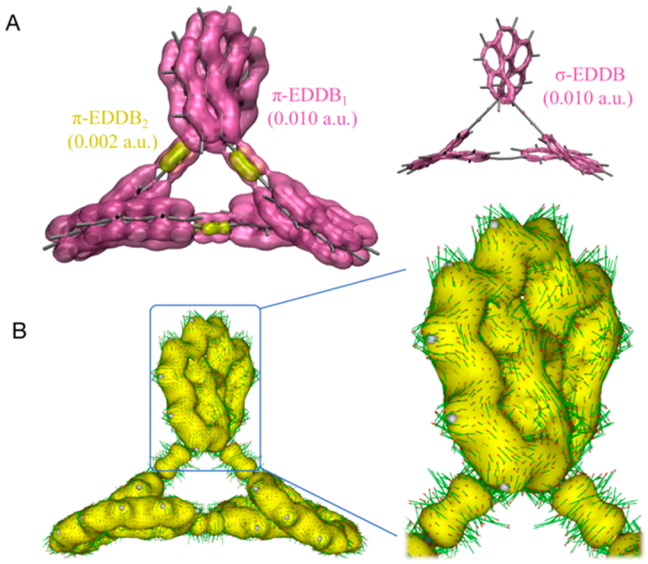

Figure 5. (A) Electron density of delocalized bonds (EDDB) of $\mathbf{2}_{PPM}$ showing π-$EDDB_1$ (45.98e, pink), π-$EDDB_2$ (0.32e, yellow), and σ-EDDB (9.06e, pink) with their isovalues labeled. (B) Anisotropy of the induced current density (ACID) plots of $\mathbf{2}_{PPM}$ showing directional electron currents within each helicene unit and nondirectional electron currents at the alkynes (isovalue 0.030 au). The external magnetic field vector is perpendicular to the ACID plots and points toward the viewer.

$EDDB_1$, pink). As expected, the p orbitals orthogonal to the helicene plane contribute negligible electron density to overall electron delocalization (Figure 5A, π-$EDDB_2$, yellow). While σ delocalization is evident within the framework of the helicene fragments, almost zero σ delocalization is observed along the bridging alkynyl bonds. Nondirectional electron currents can be observed at the alkynes in the anisotropic current (induced) density (ACID)[14] plot, showing minimal helicene−helicene interactions with no significant global aromaticity (Figure 5B). Similar results were observed for an analogous compound reported by Herges and Durola,[6a] and the authors argued that their system features global Möbius aromaticity with concurrent diatropic and paratropic ring currents. A larger extent of delocalization was observed for the T_1 excited state of **2**, resulting in an increased level of electron delocalization between the helicene and the alkyne units (Figure S27).

Chiral separation of the enantiomers of **2** was achieved by analytical HPLC with a chiral-stationary-phase column (CHIRALPAK IB-3). However, preparatory-scale separation of **2** was unsuccessful because of its limited solubility. Modification of the alkynes was attempted to address the limited solubility and electrochemical stability of macrocycle **2**. As shown in Figure 6, one of the three alkynes selectively reacts with tetrasubstituted cyclopentadienone **5**, and the Möbius topology is largely preserved in the product **6**. Subsequent cycloadditions were not observed, possibly because of the steric hindrance around the remaining alkynes. To examine the substrate scope of the reported synthetic strategy, alkyne metathesis was also attempted for two structurally related substrates. Compound **7** features an axially chiral binaphthyl structure, which was key to the Möbius structure reported by Rissanen and Herges,[6b] and hetero-

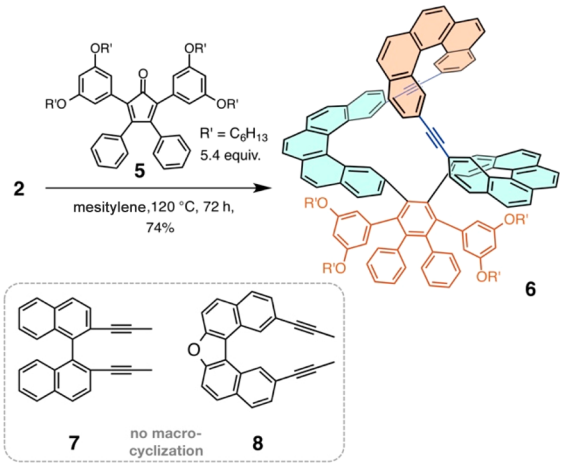

Figure 6. Cyclopentadienone **5** selectively reacted with one of the three alkynes in **2** to give compound **6** with pseudo-twofold symmetry. Compounds **7** and **8** failed to form macrocyclic oligomers.

helicene precursor **8** is structurally analogous to **1**; however, neither substrate gave any macrocycles via metathesis.

In conclusion, we have demonstrated the use of alkyne metathesis in the preparation of Möbius tris((ethynyl)[5]helicene) macrocycle **2** through a synthetically efficient cyclooligomerization process. The high diastereoselectivity results from a 15.4 kcal/mol difference in activation energy during the cyclization step in favor of the *PPM*/*MMP* diastereomer. The findings reported here shed light on the kinetic aspects of alkyne metathesis cyclooligomerization, which is different from other DCC reactions. While the lack of directional currents throughout the molecule in the ACID plot suggests a negligible global aromaticity, the alignment of p orbitals in the EDDB plots is set up for delocalization of π electrons of the helicene and acetylene units in **2**.

■ ASSOCIATED CONTENT

Supporting Information

The Supporting Information is available free of charge at https://pubs.acs.org/doi/10.1021/jacs.0c01430.

Synthesis and characterization of compounds and results of computational studies (PDF)
Crystallographic data for **2** (CIF)

■ AUTHOR INFORMATION

Corresponding Authors

Miguel A. Garcia-Garibay − *Department of Chemistry and Biochemistry, University of California, Los Angeles, California 90095, United States;* orcid.org/0000-0002-6268-1943; Email: mgg@chem.ucla.edu

Jun Zhu − *State Key Laboratory of Physical Chemistry of Solid Surfaces, Collaborative Innovation Center of Chemistry for Energy Materials, Fujian Provincial Key Laboratory of Theoretical and Computational Chemistry, Department of Chemistry, College of Chemistry and Chemical Engineering, Xiamen University, Xiamen 361005, China;* orcid.org/0000-0002-2099-3156; Email: jun.zhu@xmu.edu.cn

Jeffrey S. Moore − *Beckman Institute for Advanced Science and Technology and Department of Chemistry, University of Illinois at Urbana−Champaign, Urbana, Illinois 61801, United States; Joint Center for Energy Storage Research, Argonne, Illinois*

https://dx.doi.org/10.1021/jacs.0c01430
J. Am. Chem. Soc. XXXX, XXX, XXX−XXX

60439, United States; orcid.org/0000-0001-5841-6269; Email: jsmoore@illinois.edu

Authors

Xing Jiang − *Beckman Institute for Advanced Science and Technology, University of Illinois at Urbana−Champaign, Urbana, Illinois 61801, United States;* orcid.org/0000-0001-8259-1948

Summer D. Laffoon − *Department of Chemistry, University of Illinois at Urbana−Champaign, Urbana, Illinois 61801, United States*

Dandan Chen − *State Key Laboratory of Physical Chemistry of Solid Surfaces, Collaborative Innovation Center of Chemistry for Energy Materials, Fujian Provincial Key Laboratory of Theoretical and Computational Chemistry, Department of Chemistry, College of Chemistry and Chemical Engineering, Xiamen University, Xiamen 361005, China*

Salvador Pérez-Estrada − *Department of Chemistry and Biochemistry, University of California, Los Angeles, California 90095, United States*

Andrew S. Danis − *Department of Chemistry, University of Illinois at Urbana−Champaign, Urbana, Illinois 61801, United States; Joint Center for Energy Storage Research, Argonne, Illinois 60439, United States*

Joaquín Rodríguez-López − *Beckman Institute for Advanced Science and Technology and Department of Chemistry, University of Illinois at Urbana−Champaign, Urbana, Illinois 61801, United States; Joint Center for Energy Storage Research, Argonne, Illinois 60439, United States;* orcid.org/0000-0003-4346-4668

Complete contact information is available at: https://pubs.acs.org/10.1021/jacs.0c01430

Author Contributions

[▽]X.J., S.D.L., and D.C. contributed equally.

Notes

The authors declare no competing financial interest.

The crystallographic data for **2** are also accessible from the Cambridge Crystallographic Data Centre under deposition number CDCC 1978635.

■ ACKNOWLEDGMENTS

This work was supported with funds from the Arnold and Mabel Beckman Foundation (Postdoctoral Fellowship to X.J.), the U.S. National Science Foundation (CHE-1855342 to M.A.G.-G.; CHE-1904180 to J.S.M.; Graduate Research Fellowship Program, DGE-1746047, to S.D.L.), the Joint Center for Energy Storage Research (JCESR), an Energy Innovation Hub funded by the U.S. Department of Energy, Office of Science, Office of Basic Energy Sciences (J.S.M and J.R.-L.), the National Natural Science Foundation of China (21573179 to J.Z.), and the Top-Notch Young Talents Program of China (J.Z.). We thank Anna Yang and Chris Pattillo for helpful discussions and Lucas Hernandez and Prof. David Sarlah for the chiral HPLC analysis.

■ REFERENCES

(1) For recent books and reviews on DCC, see: (a) *Dynamic Covalent Chemistry: Principles, Reactions, and Applications*; Zhang, W., Jin, Y., Eds.; John Wiley & Sons: Chichester, U.K., 2017. (b) *Dynamic Combinatorial Chemistry*; Reek, J. N. H., Otto, S., Eds.; Wiley-VCH: Weinheim, Germany, 2010. (c) Frei, P.; Hevey, R.; Ernst, B. Dynamic Combinatorial Chemistry: A New Methodology Comes of Age. *Chem. - Eur. J.* **2019**, *25*, 60−73. (d) Rowan, S. J.; Cantrill, S. J.; Cousins, G. R. L.; Sanders, J. K. M.; Stoddart, J. F. Dynamic Covalent Chemistry. *Angew. Chem., Int. Ed.* **2002**, *41*, 898−952.

(2) (a) Hillenbrand, J.; Leutzsch, M.; Fürstner, A. Molybdenum Alkylidyne Complexes with Tripodal Silanolate Ligands: The Next Generation of Alkyne Metathesis Catalysts. *Angew. Chem., Int. Ed.* **2019**, *58*, 15690−15696. (b) Thompson, R. R.; Rotella, M. E.; Du, P.; Zhou, X.; Fronczek, F. R.; Kumar, R.; Gutierrez, O.; Lee, S. Siloxide Podand Ligand as a Scaffold for Molybdenum-Catalyzed Alkyne Metathesis and Isolation of a Dynamic Metallatetrahedrane Intermediate. *Organometallics* **2019**, *38*, 4054−4059. (c) Ehrhorn, H.; Tamm, M. Well-Defined Alkyne Metathesis Catalysts: Developments and Recent Applications. *Chem. - Eur. J.* **2018**, *25*, 3190−3208. (d) Du, Y.; Yang, H.; Zhu, C.; Ortiz, M.; Okochi, K. D.; Shoemaker, R.; Jin, Y.; Zhang, W. Highly Active Multidentate Ligand-Based Alkyne Metathesis Catalysts. *Chem. - Eur. J.* **2016**, *22*, 7959−7963. (e) Fürstner, A. Alkyne Metathesis on the Rise. *Angew. Chem., Int. Ed.* **2013**, *52*, 2794−2819.

(3) (a) Lee, S.; Yang, A.; Moneypenny, T. P., II; Moore, J. S. Kinetically Trapped Tetrahedral Cages via Alkyne Metathesis. *J. Am. Chem. Soc.* **2016**, *138*, 2182−2185. (b) Wang, Q.; Zhang, C.; Noll, B. C.; Long, H.; Jin, Y.; Zhang, W. A Tetrameric Cage with D_{2h} Symmetry through Alkyne Metathesis. *Angew. Chem., Int. Ed.* **2014**, *53*, 10663−10667.

(4) (a) Rzepa, H. S. Möbius Aromaticity and Delocalization. *Chem. Rev.* **2005**, *105*, 3697−3715. (b) Herges, R. Topology in Chemistry: Designing Möbius Molecules. *Chem. Rev.* **2006**, *106*, 4820−4842.

(5) For reviews on Möbius structures of porphyrinoids, see: (a) Stępień, M.; Sprutta, N.; Latos-Grazyński, L. Figure Eights, Möbius Bands, and More: Conformation and Aromaticity of Porphyrinoids. *Angew. Chem., Int. Ed.* **2011**, *50*, 4288−4340. (b) Saito, S.; Osuka, A. Expanded Porphyrins: Intriguing Structures, Electronic Properties, and Reactivities. *Angew. Chem., Int. Ed.* **2011**, *50*, 4342−4373. (c) Yoon, Z. S.; Osuka, A.; Kim, D. Möbius Aromaticity and Antiaromaticity in Expanded Porphyrins. *Nat. Chem.* **2009**, *1*, 113−122.

(6) (a) Naulet, G.; Sturm, L.; Robert, A.; Dechambenoit, P.; Röhricht, F.; Herges, R.; Bock, H.; Durola, F. Cyclic Tris-[5]Helicenes with Single and Triple Twisted Möbius Topologies and Möbius Aromaticity. *Chem. Sci.* **2018**, *9*, 8930−8936. (b) Schaller, G. R.; Topić, F.; Rissanen, K.; Okamoto, Y.; Shen, J.; Herges, R. Design and Synthesis of the First Triply Twisted Möbius Annulene. *Nat. Chem.* **2014**, *6*, 608−613.

(7) Nishigaki, S.; Shibata, Y.; Nakajima, A.; Okajima, H.; Masumoto, Y.; Osawa, T.; Muranaka, A.; Sugiyama, H.; Horikawa, A.; Uekusa, H.; Koshino, H.; Uchiyama, M.; Sakamoto, A.; Tanaka, K. Synthesis of Belt- and Möbius-Shaped Cycloparaphenylenes by Rhodium-Catalyzed Alkyne Cyclotrimerization. *J. Am. Chem. Soc.* **2019**, *141*, 14955−14960.

(8) Heilbronner, E. Hückel Molecular Orbitals of Möbius-Type Conformations of Annulenes. *Tetrahedron Lett.* **1964**, *5*, 1923−1928.

(9) Ajami, D.; Oeckler, O.; Simon, A.; Herges, R. Synthesis of a Möbius Aromatic Hydrocarbon. *Nature* **2003**, *426*, 819−821.

(10) Jhulki, S.; Mishra, A. K.; Chow, T. J.; Moorthy, J. N. Helicenes as All-in-One Organic Materials for Application in OLEDs: Synthesis and Diverse Applications of Carbo- and Aza[5]Helical Diamines. *Chem. - Eur. J.* **2016**, *22*, 9375−9386.

(11) (a) Gingras, M.; Félix, G.; Peresutti, R. One Hundred Years of Helicene Chemistry. Part 2: Stereoselective Syntheses and Chiral Separations of Carbohelicenes. *Chem. Soc. Rev.* **2013**, *42*, 1007−1050. (b) Goedicke, C.; Stegemeyer, H. Resolution and Racemization of Pentahelicene. *Tetrahedron Lett.* **1970**, *11*, 937−940. (c) Berezhnaia, V.; Roy, M.; Vanthuyne, N.; Villa, M.; Naubron, J.-V.; Rodriguez, J.; Coquerel, Y.; Gingras, M. Chiral Nanographene Propeller Embedding Six Enantiomerically Stable [5]Helicene Units. *J. Am. Chem. Soc.* **2017**, *139*, 18508−18511.

(12) Legault, C. Y. *CYLview*, ver. 1.0b; Université de Sherbrooke, 2009; http://www.cylview.org.

https://dx.doi.org/10.1021/jacs.0c01430
J. Am. Chem. Soc. XXXX, XXX, XXX−XXX

(13) (a) Shen, M.; Rodríguez-López, J.; Lee, Y.-T.; Chen, C.-T.; Fan, F.-R. F.; Bard, A. J. Electrochemistry and Electrogenerated Chemiluminescence of a Novel Donor-Acceptor FPhSPFN Red Fluorophore. *J. Phys. Chem. C* **2010**, *114*, 9772−9780. (b) Shen, M.; Rodríguez-López, J.; Huang, J.; Liu, Q.; Zhu, X.-H.; Bard, A. J. Electrochemistry and Electrogenerated Chemiluminescence of Dithienylbenzothiadiazole Derivative. Differential Reactivity of Donor and Acceptor Groups and Simulations of Radical Cation-Anion and Dication-Radical Anion Annihilations. *J. Am. Chem. Soc.* **2010**, *132*, 13453−13461.

(14) Geuenich, D.; Hess, K.; Köhler, F.; Herges, R. Anisotropy of the Induced Current Density (ACID), a General Method to Quantify and Visualize Electronic Delocalization. *Chem. Rev.* **2005**, *105*, 3758−3772.

https://dx.doi.org/10.1021/jacs.0c01430
J. Am. Chem. Soc. XXXX, XXX, XXX−XXX